Calculating the many-body density of states on a digital quantum computer

Alessandro Summer[1,2,*] Cecilia Chiaracane[1,†] Mark T. Mitchison,[1,2,‡] and John Goold[1,2,3,§]
[1]*School of Physics, Trinity College Dublin, Dublin 2, Ireland*
[2]*Trinity Quantum Alliance, Unit 16, Trinity Technology and Enterprise Centre, Pearse Street, Dublin 2, D02 YN67, Ireland*
[3]*Algorithmiq Limited, Kanavakatu 3C 00160 Helsinki, Finland*

(Received 11 April 2023; accepted 15 December 2023; published 26 January 2024)

Quantum statistical mechanics allows us to extract thermodynamic information from a microscopic description of a many-body system. A key step is the calculation of the density of states, from which the partition function and all finite-temperature equilibrium thermodynamic quantities can be calculated. In this work, we devise and implement a quantum algorithm to perform an estimation of the density of states on a digital quantum computer which is inspired by the kernel polynomial method. Classically, the kernel polynomial method allows us to sample spectral functions via a Chebyshev polynomial expansion. Our algorithm computes moments of the expansion on quantum hardware using a combination of random-state preparation for stochastic trace evaluation and a controlled unitary operator. We use our algorithm to estimate the density of states of a nonintegrable Hamiltonian on the Quantinuum H1-1 trapped ion chip for a controlled register of 18 qubits. This not only represents a state-of-the-art calculation of thermal properties of a many-body system on quantum hardware, but also exploits the controlled unitary evolution of a many-qubit register on an unprecedented scale.

DOI: 10.1103/PhysRevResearch.6.013106

I. INTRODUCTION

The idea of using one quantum system to efficiently simulate another one was the vision of Feynman over 40 years ago [1]. This paradigm is known as quantum simulation [2–5] and is expected to be one of the first real applications of the current generation of quantum computers [6]. In particular, recent progress has been made in simulating the dynamics of strongly correlated many-body systems on current devices [7–11], albeit with systems which are still too small to compete with calculations on classical supercomputing architectures. The hope is that the achievable system sizes will eventually become large enough to surpass what is classically possible.

In terms of using quantum simulators to extract eigenenergies of many-body systems, early ideas include algorithms based on quantum Fourier transform [12] such as quantum phase estimation [12–14] and adiabatic state preparation [15]. The development of algorithms for the extraction of ground-state energies is central for the promise of being able to perform quantum chemistry and materials simulations on quantum computers [16–19] and ground state energy calculation is a target of many variational quantum algorithms [20,21]. Results for finite temperature and excited states are more scarce. However, recent proposals to measure finite temperature expectation values on hardware include sampling [22–24] and imaginary time evolution [25], and more recently algorithms which may have potential for computing microcanonical expectation values were proposed in Ref. [26].

The more general idea of using quantum computers to do statistical mechanics is a topic which is gaining traction [26,27]. In this work we focus on developing an algorithm that gives a coarse-grained estimate of the density of states (DOS) based on the classical kernel polynomial method (KPM) [28]. The KPM provides a reconstruction of a spectral function by means of a Chebyshev polynomial expansion, weighted by suitable kernels to damp the Gibbs oscillations that occur due to finite series truncation. Chebyshev moments are computed iteratively by applying functions of the Hamiltonian on some initial state. This step is a challenge to implement on quantum hardware.

Block encoding of a Hamiltonian is deeply connected with the Chebyshev polynomials [29], implementing the Hamiltonian as a quantum walk as exploited in the context of the KPM in Ref. [30] and more generally to estimate physical properties in Refs. [31,32]. Alternatives are to compute the Chebyshev moments iteratively in a variational quantum algorithm [33] or to overcome the problem of implementing the Chebyshev polynomials using suitably defined Fourier ones [34,35].

In this work we devise a hybrid algorithm which uses a combination of pseudorandom-state preparation, Hadamard test, and Suzuki-Trotter (ST) decomposition [36] to evaluate Chebyshev moments. These moments are then used in the standard KPM expansion. We use an arccosine approximation of the Hamiltonian to implement Chebyshev polynomials from standard ST decomposition and implement our algo-

*summera@tcd.ie
†chiaracc@tcd.ie
‡mark.mitchison@tcd.ie
§gooldj@tcd.ie

rithm on the Quantinuum H1-1 trapped ion quantum simulator [37]. We were able to approximate the DOS of a nonintegrable spin chain for up to 18 qubits using a single ancillary qubit. Our simulations represent one of the first explorations of the use of near-term quantum computers for calculations in statistical mechanics.

In Sec. II we introduce the KPM method and discuss its use in the context of statistical mechanics. We discuss how to compute the DOS and how a pseudorandom state can be used for stochastic trace estimation. In Sec. III we explain the quantum algorithm for extracting Chebyshev polynomials and discuss the subroutines for random-state preparation and implementing the arccosine approximation of the Hamiltonian. In Sec. IV we then introduce the model we simulate on hardware and the corresponding gate decomposition used to implement the controlled unitary. We display our results for estimations of DOS computed using our hybrid algorithm for systems sizes of 12 and 18 qubits.

II. CLASSICAL KERNEL POLYNOMIAL METHOD FOR THE DENSITY OF STATES

A. Density of states

In this section we give an overview of the classical KPM and discuss how it is used to calculate the DOS [28]. The DOS of a system of L qubits described by the Hamiltonian $\hat{H}$ is defined as

$$g(E) = \frac{1}{2^L}\sum_{k=0}^{2^L-1}\delta(E - E_k), \tag{1}$$

where E_k are the energy eigenvalues, and $|k\rangle$ the corresponding eigenvectors, i.e., $\hat{H}\,|k\rangle = E_k\,|k\rangle$. The DOS gives access to all thermodynamic properties; in particular, the canonical partition function can be evaluated as

$$\mathcal{Z}(\beta) = \int e^{-\beta E} g(E) dE, \tag{2}$$

and from $\mathcal{Z}(\beta)$, the energy

$$E(\beta) = -\frac{\partial[\ln \mathcal{Z}(\beta)]}{\partial\beta} \tag{3}$$

and the entropy $S(\beta) = \beta[E(\beta) - F(\beta)]$, with $F(\beta) = -\beta^{-1}\ln[\mathcal{Z}(\beta)]$ the free energy.

In order to extract the DOS from a system of size L one would typically need exact diagonalization, which requires memory resources scaling as $O(2^{3L})$. In contrast, the KPM described in the following section is able to approximate the DOS with memory scaling as $O(2^L)$ when combined with a stochastic evaluation of the trace, as analysed in Sec. II D.

B. Kernel polynomial method

We consider a function $f(x)$ defined on the interval $x \in [-1, 1]$. The KPM provides an approximation of this function by a finite series of M Chebyshev polynomials. Mathematically, it is given by

$$f_{\mathrm{KPM}}(x) = \frac{1}{\pi\sqrt{1-x^2}}\left[\gamma_0^M\mu_0 + 2\sum_{m=1}^{M}\gamma_m^M\mu_m T_m(x)\right], \tag{4}$$

where γ_m^M are the kernel coefficients used to damp Gibbs oscillations, $T_m(x)$ the Chebyshev polynomials, and μ_m the Chebyshev moments. While a more detailed discussion can be found in Appendix A, the Chebyshev polynomials are defined as

$$T_m(x) = \cos[m\arccos(x)], \quad \text{with } m \in \mathbb{N}_0, \tag{5}$$

and obey the following recursion relation,

$$T_m(x) = 2xT_{m-1}(x) - T_{m-2}(x), \tag{6}$$

where $T_0(x) = 1$, $T_1(x) = x$. The KPM expansion in Eq. (4) is thus reconstructed by computing the corresponding Chebyshev moments

$$\mu_m(x) = \int_{-1}^{1} f(x)T_m(x)dx. \tag{7}$$

The KPM can be adapted to estimate general spectral functions related to a given quantum mechanical Hamiltonian. In this work, we use it to get an estimate of the DOS. We note that recently the KPM has been implemented using tensor network techniques [38], and was adopted to study thermalization [39] as well as to extract the DOS of simple models in lattice gauge theory [40]. One clear advantage of the KPM is that it does not suffer from the sign problem that is synonymous with Monte Carlo simulations.

C. Chebyshev moments of the DOS

In this section we discuss the key steps in computing the KPM approximation of the DOS, $D(E)$. Since the domain of the Chebyshev polynomials is the interval $[-1, 1]$, $\hat{H}$ must have a spectral norm $||\hat{H}|| \leqslant 1$. If not, $\hat{H}$ can be normalized as

$$\hat{H} \mapsto \frac{\hat{H} - \mathrm{a}}{\mathrm{b}}, \tag{8}$$

with

$$\mathrm{a} := \frac{E_{\max} + E_{\min}}{2} \quad \text{and} \quad \mathrm{b} := \frac{E_{\max} - E_{\min}}{2 - \varepsilon}, \tag{9}$$

where $E_{\max}$ and $E_{\min}$ are the largest and smallest eigenvalues of $\hat{H}$. Additionally, a small cutoff ε is introduced to avoid stability issues that can arise close to the boundaries of the spectrum. After the rescaling, the expression for the moments μ_m becomes

$$\begin{aligned}\mu_m &:= \int_{-1}^{1} D(E)T_m(E)dE \\ &= \int_{-1}^{1}\frac{1}{2^L}\sum_{k=0}^{2^L-1}\delta(E - E_k)T_m(E)dE \\ &= \frac{1}{2^L}\sum_k T_m(E_k) = \frac{1}{2^L}\sum_k \langle k|\, T_m(\hat{H})\,|k\rangle \\ &= \frac{1}{2^L}\mathrm{Tr}[T_m(\hat{H})].\end{aligned} \tag{10}$$

D. Stochastic trace evaluation

The first task in the extraction of Chebyshev moments in the KPM is the efficient estimation of the trace in Eq. (10).

Given an operator $\hat{X}$ acting on L qubits, determining all the elements $X_{ii} := \langle i|\hat{X}|i\rangle$ in its trace requires $O(2^{2L})$ operations [41]. A common alternative method to this computational procedure is stochastic trace estimation. The main idea is to estimate $\hat{X}$ on a set of randomly chosen states. Let $\{|r\rangle\}$ be a set of R random states on L qubits,

$$|r\rangle = \sum_{i=0}^{2^L-1} c_{ri}|i\rangle \quad \text{with } c_{ri} \in \mathbb{C}, \tag{11}$$

and the stochastic estimate

$$\Theta = \frac{1}{R}\sum_r \langle r|\hat{X}|r\rangle . \tag{12}$$

If the coefficients fulfill the following conditions,

$$\langle\langle c_{ri}\rangle\rangle = 0, \tag{13}$$

$$\langle\langle c_{ri}c_{r'j}\rangle\rangle = 0, \tag{14}$$

$$\langle\langle c^*_{ri}c_{r'j}\rangle\rangle = \delta_{rr'}\delta_{ij}, \tag{15}$$

where $\langle\langle\cdot\rangle\rangle$ indicates the statistical average over i, then the variance in the estimate of $\mathrm{Tr}[\hat{X}]$ is

$$(\delta\Theta)^2 = \frac{1}{R}\left(\mathrm{Tr}[\hat{X}^2] + (\langle\langle|c_{ri}|^4\rangle\rangle - 2)\sum_{j=0}^{2^L-1} X_{jj}^2\right) \tag{16}$$

(for more details see Ref. [28]). Therefore, the relative error scales as $O(1/\sqrt{R2^L})$, which implies that fewer random states will be needed to achieve a fixed level of precision as the size of the system increases. Note that if the coefficients of the random states are distributed as a Gaussian, then the variance of Θ only depends on $\mathrm{Tr}[\hat{X}^2]$.

The stochastic trace is used in conjunction with the recursion relation in Eq. (6) to estimate the Chebyshev moments. Starting from a random state $|r\rangle = |r_0\rangle$, one can define

$$|r_1\rangle = \hat{H}|r_0\rangle , \tag{17}$$

and recursively generate a series of M vectors

$$|r_m\rangle = 2\hat{H}|r_{m-1}\rangle - |r_{m-2}\rangle = T_m(\hat{H})|r\rangle . \tag{18}$$

The moments can then be obtained from the overlap $\langle r_m|r\rangle = \langle r|T_m(\hat{H})|r\rangle$.

A potential issue of computing the moments in this way is that it makes the precision of the mth moment dependent on errors from the evaluation of the previous ones. As mentioned earlier, the computation of the moments is the major bottleneck of the classical KPM method, limiting the size of the systems it can be applied to. In the next section we describe our algorithm to compute the mth Chebyshev moment on a quantum computer.

III. KERNEL POLYNOMIAL METHOD HYBRID QUANTUM ALGORITHM

In Fig. 1 we show the circuit used to compute Chebyshev moments on quantum hardware. Our proposal is reminiscent of the DQC1 protocol [42], which is a subuniversal computational paradigm that requires $L+1$ qubits to estimate the real or imaginary part of the trace of a unitary operator acting on L qubits. L qubits are initialized in the maximally mixed state while the remaining clean one acts as a control qubit of a Hadamard test [43] applied on the whole register, similarly as in Fig. 1. On a digital quantum computer, where states are considered to be ideally pure, the maximally mixed state can be approximated by random states. The initialization of the L qubits in the maximally mixed state is responsible for the subuniversality of the model [44]. However, the protocol still enables potential exponential quantum speedup [45] and it is strongly believed that no classical method can simulate it efficiently [46,47].

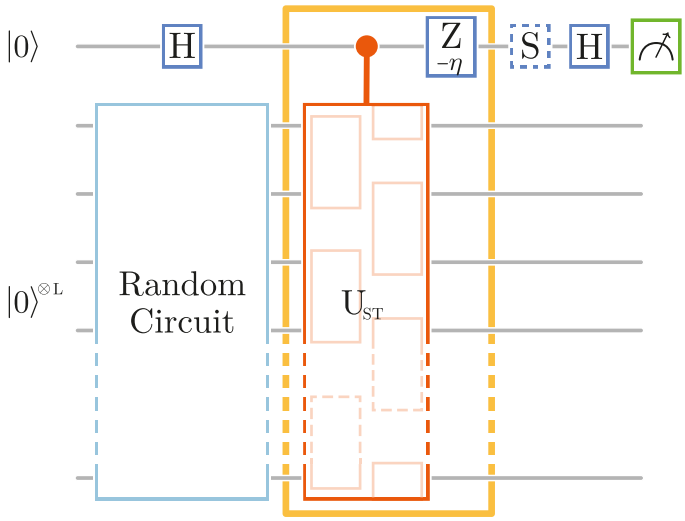

FIG. 1. Proposed circuit for the computation of Chebyshev moments on the quantum computer. A pseudorandom state is generated by means of a random circuit on a register of L qubits and an ancillary qubit is prepared in the $|+\rangle$ state with a Hadamard operation. A unitary operation $e^{im\hat{H}_K}$ is then performed on the register and controlled on the ancillary qubit (yellow rectangular). This is pursued through a controlled unitary and a rotation Z, with η the coefficient of the identity in $\hat{H}_K$. The subsequent gates and measurements on the controlled qubit yield $\mathrm{Tr}[\cos(m\hat{H}_K)]$ and $\mathrm{Tr}[\sin(m\hat{H}_K)]$, where $\hat{H}_K$ is connected to the arc-cosine expansion defined by Eq. (39) and then to the mth-order Chebyshev polynomial of the Hamiltonian.

On current hardware, the implementation of the control unitary operator for the Hadamard test still faces certain limitations. There are two main reasons for this. First, it requires connecting each Pauli operator of the Hamiltonian to the control qubit, which can be challenging for devices with limited connectivity. Second, controlling the evolution operator of a k-local Hamiltonian results in a $(k+1)$-local operator, leading to an increase in the number of two-qubit gates required. We discuss our strategy to optimize the gate count for our specific problem in Fig. 6. Additionally, the all-to-all connectivity of the Quantinuum H1-1 device used here avoids the issues related to the first problem. For devices with more limited connectivity a delocalization of the control qubit seems necessary, namely controlling the unitary operator of the Hadamard test from more qubits at the same time. This can be done by creating a GHZ state through different qubits that one wants to treat as controllers of the local neighborhood of qubits around them, as in Fig. 2.

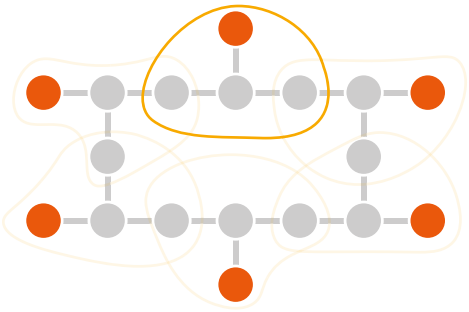

FIG. 2. Delocalization of the control qubit for a chain of $L = 12$ qubits using the heavy-hex mapping. The 6 orange qubits serve as controls for the L gray qubits. If the Hamiltonian exhibits only nearest-neighbor interactions, each control qubit can efficiently govern two pairs of qubits (shown with the yellow paths), requiring no SWAP operations.

In the following, we discuss the two main parts of the circuit in detail. In Sec. III A we analyze the random circuit we use to mimic the maximally mixed state and in Sec. III B the application of the controlled unitary for the extraction of the Chebyshev moments.

A. Stochastic trace evaluation via state randomization

The generation of random states on quantum computers has recently garnered considerable attention due to their important role in benchmarking [48]. However, producing uniformly random states that sample the Haar distribution is inefficient, as the number of required gates scales exponentially with the register size [49,50]. T designs are a type of circuit that replicate moments of the Haar distribution up to order T or lower [51]. They offer some improvement in terms of gate efficiency, with the number of required gates scaling polynomially with the number of qubits. Nonetheless, exact T designs are still costly and may be overly random for specific purposes [52]. Here we take an alternative approach based on pseudorandom-state generation [50]. This involves the generation of states that do not uniformly sample the Haar distribution [53], but still possess the desired properties such as Eqs. (13) and (14). This method has been shown to generate states that are sufficiently random in an efficient way.

Using pseudorandom states to stochastically evaluate the trace has been proposed in various papers [34,54–58], and recently used on quantum hardware to extract high-temperature transport exponents [11]. In order to generate pseudorandom states, one can use a circuit composed of alternating layers of 2-qubit gates and layers with random single-qubit rotations, as suggested by Ref. [50] and adopted in Refs. [11,48,54] with small variations.

This random composition has become a widely accepted method for generating this type of random state. In Ref. [54] the random state is aimed at generation on a quantum computer where the qubits are connected in a ring geometry. Layers of 2-qubit gates connecting even-odd and odd-even qubits are alternated and in between them, there are layers of single-qubit gates randomly chosen among $\{\hat{X}(\pi/2), \hat{Y}(\pi/2), \hat{Z}(\pi/4)\}$ so that the same rotation is not applied to the same qubit sequentially.

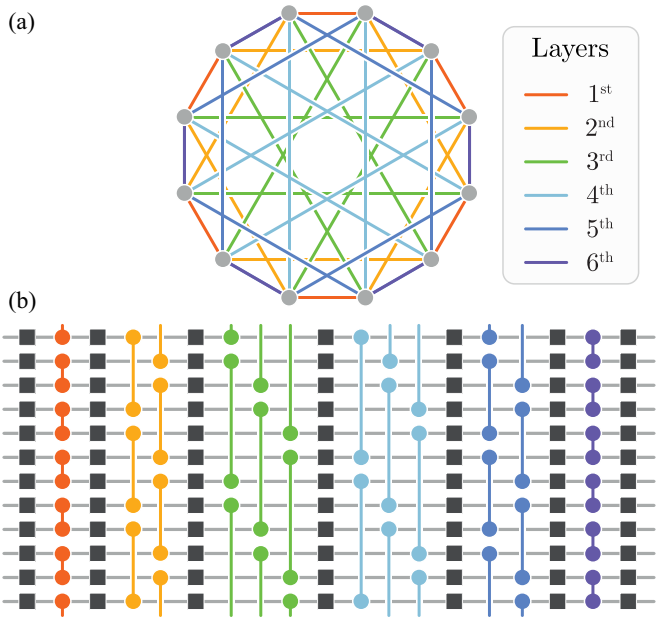

FIG. 3. The 6-layer randomized circuit used for trace evaluation at $L = 12$ (the blue box on the L-1 qubit register in Fig. 1). (a) A graphical representation of the circuit connectivity: the gray dots represent the qubits, and the colored lines are the 2-qubit gates numbered according to the order of application. Note that this particular structure is chosen to exploit the all to all connectivity of the Quantinuum H1-1 device [37]. (b) Gate decomposition of the random circuit. The colored lines represent $\hat{Z}\hat{Z}(\pi/2)$ gates, and the dark gray squares are single-qubit rotations, randomly selected from $\hat{X}(\pi/2)$, $\hat{Y}(\pi/4)$, and $\hat{Z}(\pi/2)$. The latter two will be removed by the compilation since they commute with $\hat{Z}\hat{Z}(\pi/2)$ and anticommute with the other operators. Therefore, their effect is to add two more types of single-qubit rotations.

In our case, we focus on a variation of this procedure that takes advantage of the all-to-all connectivity and of the specific set of elementary gates that can be implemented directly on the Quantinuum H1-1 trapped-ion-based quantum computer (see Fig. 3). The gate set of the Quantinuum H1-1 device includes

$$\begin{aligned} \hat{Z}\hat{Z}(\theta) &= e^{-i\theta/2\hat{Z}\otimes\hat{Z}}, \\ \hat{Z}(\theta) &= e^{-i\theta/2\hat{Z}}, \\ \hat{U}_{1q}(\theta,\phi) &= e^{-i\theta/2[\cos(\phi)\hat{X}+\sin(\phi)\hat{Y}]}. \end{aligned} \tag{19}$$

The device that we will use also supports parallelization (using quantum charge-coupled device (QCCD) architecture with five parallel gate zones [59]). Inspired by existing techniques to create shallow randomizers, we change the single-qubit rotations to be chosen from $\{\hat{X}(\pi/2), \hat{Y}(\pi/4), \hat{Z}(\pi/2)\}$. Note that the former two rotations can be applied as a single $\hat{U}_{1q}(\theta,\phi)$ gate, while the latter can be implemented virtually [60]. The 2-qubit gate will now be a $\hat{Z}\hat{Z}(\pi/2)$ with a different connectivity. Each $\hat{Z}\hat{Z}(\pi/2)$ will connect the qubits $2i$ and $(2i+p) \mod L$ with $i = 0, \ldots, L/2$ and p an odd number called a *jump*. The jumps are chosen so that each qubit is narrowly connected to the other. For instance, as shown in Fig. 3, the jumps of the first half of the layers can be chosen

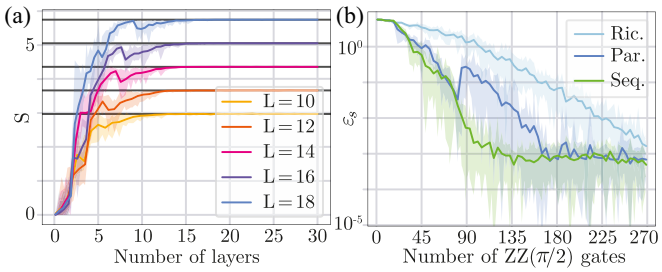

FIG. 4. The convergence of different half-chain entanglement entropies to the expected value, for $L = 10, 12, 14, 16$, and 18 averaged over 20 different random states. The shadows are drawn by the values of the individual random states. (a) The half-chain von Neumann entropy S is shown as a function of random circuit depth and shows the saturation to the Page value [61] (dark gray lines) for different system size for the circuit used in this work (Par.). (b) Comparison of the relative error of the von Neumann half-chain entropy ε_s at $L = 18$ of the three different random circuits: the one proposed in Richter *et al.* [54] (Ric.), the one used in this work (Par.) (see Fig. 3), and one where the 2-qubit gates are applied sequentially (Seq.). All three circuits lead to fast convergence to a maximally bipartite entangled state. We note that the relative error in Seq. seems to be most favorable but we have used Par. on the hardware here because fewer layers are required to get a good estimate of the trace.

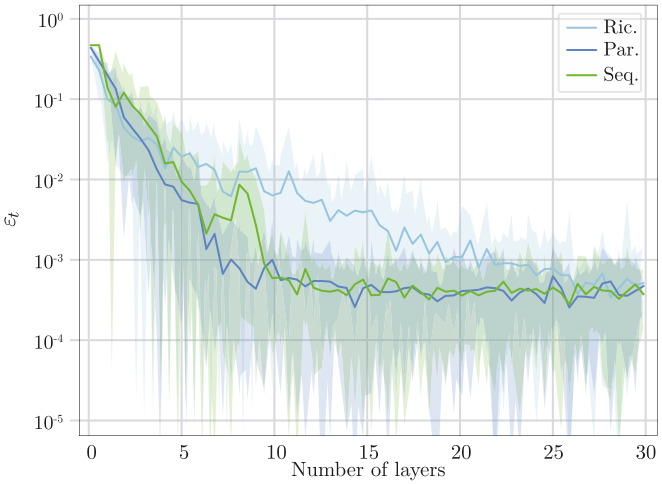

FIG. 5. Convergence of relative error ε_t of the stochastic trace to the trace of the Hamiltonian defined by Eq. (48) with $L = 18$ for the three random circuits used to generate Fig. 4. The results are averaged over 20 different random states from which the shadows are obtained.

with $p_\ell = -(-1)^\ell(2s\ell + 1)$ with $s \in \mathbb{N}_0$ and ℓ the index of the layer, and with $p_\ell = -p_{-\ell}$ for the second half of the layers. In particular, Fig. 3 shows the random compiler with $L = 12$ and $s = 1$. Notice that $s = 0$ reproduces the same pattern of 2-qubit gates as in [54].

Following Ref. [54], we quantify the randomizing effect of our circuit by checking how well the half-system entanglement entropy converges to the Page value [61], which is the entanglement entropy for a typical Haar-random state. The von Neumann entanglement entropy of a state $\rho_r = |r\rangle\langle r|$ on a space divided in subspaces $\mathcal{H}_a$ and $\mathcal{H}_b$ is

$$S(\rho_{r(a)}) = -\mathrm{Tr}[\rho_{r(a)} \ln \rho_{r(a)}] \tag{20}$$

with $\rho_{r(a)} = \mathrm{Tr}_{(b)}[|r\rangle\langle r|]$. As shown in Ref. [61], this value converges to the Page value $\ln(\dim \mathcal{H}_a) - \dim \mathcal{H}_a/(2 \dim \mathcal{H}_b)$ for random pure states. For $\dim \mathcal{H}_a = \dim \mathcal{H}_b$, it becomes $\ln(2^{L/2}) - 1/2$.

In Fig. 4, we present a classical simulation comparing the convergence rates to the Page value of three different approaches: Ric., which is the approach suggested by Richter *et al.* [54]; Par., the approach used in this work; and Seq., a variation of Par. where the 2-qubit gates are applied as a chain. In this last method, the layers of 2-qubit gates are composed of a sequence of gates; each of these has support overlapping over half of the previous and half of the succeeding gate. Therefore, we will compare these three methods in terms of the number of 2-qubit gates used instead of the number of layers. Although this last constraint limits the implementation on Quantinuum's hardware, it is helpful in analyzing the three different random compilers. In fact, while Par. is not the fastest at converging to the Page value, it performs best at estimating the trace, as shown in Fig. 5. In contrast, the states produced by Seq. converge to the Page value the fastest, but they are not as effective for trace estimation as those built with Par. This suggests that the entanglement entropy alone is not sufficient to determine a suitable state for stochastic trace estimation. In fact, we have observed that, as the entropy converges to the Page value, the fourth moment of the coefficients c_{ri} converges to 2 [as required by Eq. (16)]. This suggests that the states become Gaussian-distributed at the same rate as they approach the Page value.

The shot-noise intrinsic feature of quantum computers ultimately limits the precision of the final measurements. This limits the power of stochastic trace estimation, where even if for larger systems, as described, one single random state is enough on classical computers to achieve a sensible precision, when it is performed on quantum computers we would still need to run the circuit many times to create reliable statistics from which to extract the probability. This leads to the paradoxical outcome where random bit strings, except for particular cases, are able to achieve the same precision of typical states, since the overall error is still dominated by the shot noise. Moreover, the randomization of the states can be left to the quantum computer itself by operating a Hadamard gate followed by a measurement on a qubit initialized in $|0\rangle$, flipping the qubit only with a probability of $1/2$. Unfortunately, operating midcircuit measurements became available on Quantinuum's devices only after the ideation of this algorithm. Nevertheless, as mentioned, the performances of typical states are met by random bit strings only in some instances. In case an amplitude amplification [62] is included, for example, in the circuit, typical states still are useful.

B. Implementing the Chebyshev polynomials

Simulating the unitary evolution operator or other functions of the Hamiltonian are central tasks in the field of quantum simulation. In recent years there has been significant progress, with various approximations, like qDrift [63–66], LCU [67], Taylor expansion [68,69], and qubitization [70,71]. Importantly, the last method has been demonstrated to ex-

hibit the most favorable asymptotic scaling in terms of the number of gates required to reproduce the unitary evolution operator of a Hamiltonian. This section briefly introduces this technique before discussing an approximation that enables a rough version of it to be implemented on current devices. Qubitization relies on a routine of operators that naturally generates Chebyshev polynomials. However, plain qubitization remains challenging for NISQ devices, as seen in Ref. [72]. Therefore, extensive use of this method is still prohibitive.

The backbone of qubitization are two operators: *select* ($\hat{S}$) and *prepare* ($\hat{P}$). Consider a normalized Hamiltonian that can be decomposed into a sum of unitary operators as

$$\hat{H} = \sum_{p=1}^{P} \omega_p \hat{H}_p \quad \text{with } \hat{H}_p^2 = \hat{I} \text{ and } \omega_p \in \mathbb{R}. \tag{21}$$

The select operator is defined as

$$\hat{S} \coloneqq \sum_{p=1}^{P} |p\rangle\langle p|_{(a)} \otimes (\hat{H}_p)_{(s)}, \tag{22}$$

where (a) denotes an ancillary Hilbert space comprising a qubits, where $a \geqslant \lceil \log_2 P \rceil$ [71]. The prepare operator acts as

$$\hat{P} : |0\rangle_{(a)} \mapsto \sum_{p=1}^{P} \sqrt{\omega_p}\, |p\rangle_{(a)} =: |P\rangle_{(a)}\,. \tag{23}$$

These operators can be combined to obtain a block encoding of the Hamiltonian as

$$\langle P|_{(a)}\, \hat{S}\, |P\rangle_{(a)} = \hat{H}. \tag{24}$$

The idea behind qubitization is to exploit the block encoding of $\hat{H}$ in a quantum walk to generate any function of $\hat{H}$. The *walk operator* is defined as

$$\begin{aligned} \hat{W} &\coloneqq \underbrace{(2|P\rangle\langle P| - \hat{I})_{(a)}}_{\hat{R}_{(a)}} \hat{S} \\ &= \sum_{p,q} (2\sqrt{\omega_p \omega_q}|q\rangle\langle p| - |p\rangle\langle p|)_{(a)} \otimes (\hat{H}_p)_{(s)}, \end{aligned} \tag{25}$$

where the operator $\hat{R}_{(a)}$ acts as a reflection about the $|P\rangle$ state. The walk operator can be decomposed as

$$\begin{aligned} \hat{W} &= \bigoplus_k \begin{pmatrix} E_k & \sqrt{I - |E_k|^2} \\ -\sqrt{I - |E_k|^2} & E_k \end{pmatrix} \\ &= \bigoplus_k e^{i\hat{Y}_{(k)} \arccos E_k}, \end{aligned} \tag{26}$$

where E_k are the eigenvalues (with respective eigenstates $|k\rangle$) of $\hat{H}$ and each term of the direct sum acts on the subspace $\mathcal{H}_k$ generated by $|\phi_k\rangle \coloneqq |P\rangle\,|k\rangle$ and its orthogonal state $|\phi_k^\perp\rangle \propto (\hat{S} - E_k\hat{I})\,|\phi_k\rangle$. Likewise the $\hat{Y}_{(k)}$ operator will act as a Pauli $\hat{Y}$ operator on this subspace. Equation (26) is also useful to understand how $\hat{W}$ is isomorphic to

$$e^{i\hat{Y} \otimes \arccos \hat{H}} = \begin{pmatrix} \hat{H} & \sqrt{\hat{I} - \hat{H}^2} \\ -\sqrt{\hat{I} - \hat{H}^2} & \hat{H} \end{pmatrix}, \tag{27}$$

that is the minimal block encoding of $\hat{H}$. A fundamental feature of $\hat{W}$, on which the efficiency of qubitization is based, is that repeating it m times and projecting it on $|P\rangle$ generates the Chebyshev polynomials:

$$\langle P|_{(a)}\, \hat{W}^m\, |P\rangle_{(a)} = T_m(\hat{H}). \tag{28}$$

Let us now consider the smallest decomposition of $\hat{H}$ in unitaries, where Eq. (26) becomes easier to interpret. Given any Hamiltonian $\hat{H}$, there is a unitary operator $\hat{U}_H$ such that

$$\hat{H} = \tfrac{1}{2}(\hat{U}_H + \hat{U}_H^\dagger), \tag{29}$$

where

$$\hat{U}_H \coloneqq \sum_k e^{i \arccos E_k} |k\rangle\langle k| = e^{i \arccos \hat{H}}. \tag{30}$$

It can be observed that $\hat{U}_H^2 \neq \hat{I}$ as would seem to be required by Eq. (21); however, we notice that this condition can be relaxed by introducing a new walk operator $\hat{V} \coloneqq \hat{R}_{(a)}\hat{S}^\dagger$ and alternating it with $\hat{W}$.

As shown in detail in Appendix F, an alternative decomposition to Eq. (29) is

$$\hat{H} = \frac{1}{2i}(e^{i \arcsin \hat{H}} - e^{-i \arcsin \hat{H}}). \tag{31}$$

For the decomposition of $\hat{H}$ in Eq. (29), the prepare operator simplifies to

$$\hat{P} : |0\rangle_{(a)} \mapsto \frac{1}{\sqrt{2}} |0\rangle_{(a)} + \frac{1}{\sqrt{2}} |1\rangle_{(a)} = |+\rangle_{(a)}\,, \tag{32}$$

while the select operator becomes

$$\hat{S} = e^{i\hat{Z}_{(a)} \otimes \arccos \hat{H}_{(s)}} = \begin{pmatrix} \hat{U}_H & 0 \\ 0 & \hat{U}_H^\dagger \end{pmatrix}. \tag{33}$$

The reflection operator becomes

$$\hat{R}_{(a)} = (2|+\rangle\langle +| - \hat{I})_{(a)} = \hat{X}_{(a)}, \tag{34}$$

and the walk operators can be constructed as

$$\hat{W} = \begin{pmatrix} 0 & \hat{U}_H \\ \hat{U}_H^\dagger & 0 \end{pmatrix}, \quad \hat{V} = \begin{pmatrix} 0 & \hat{U}_H^\dagger \\ \hat{U}_H & 0 \end{pmatrix}. \tag{35}$$

The isomorphism between $\hat{W}$ and Eq. (27) is now clear since it results in mapping the ancilla from $\hat{Z}$ to $\hat{Y}$. The quantum walk now generates

$$\langle +|_{(a)} \underbrace{\ldots \hat{V}\hat{W}\hat{V}\hat{W}}_{m \text{ walk operators}} |+\rangle_{(a)} = T_m(\hat{H}). \tag{36}$$

Finally, we notice that

$$\hat{X}_{(a)}\hat{S}^\dagger\hat{X}_{(a)} = \hat{S}. \tag{37}$$

Therefore, the iteration of the select operator already generates the desirable walk:

$$\langle +|_{(a)}\, \hat{S}^m\, |+\rangle_{(a)} = T_m(\hat{H}). \tag{38}$$

We now want to utilize the decomposition in order to exploit it for the evaluation of the DOS via our KPM inspired algorithm. The KPM generally works better at the center of the Hamiltonian spectrum, where exponentially many states reside. Close to the spectral edges it can become unstable, particularly at smaller system size, and hence less reliable [28].

Exploiting the fact that exponentially many eigenstates are at the center of the spectrum, one can expand the $\arccos(\hat{H})$ around $E_k = 0$:

$$\arccos(\hat{H}) = \frac{\pi}{2} - \sum_{k=0}^{\infty} \frac{(2k)!}{2^{2k}(k!)^2(2k+1)} \hat{H}^{2k+1} = \lim_{K\to\infty} \Bigg[\frac{\pi}{2} - \underbrace{\sum_{k=0}^{K} c_k \hat{H}^{2k+1}}_{\hat{H}_K} \Bigg]. \tag{39}$$

It follows that the select operator (now depending on K) becomes

$$\hat{S}_K = e^{i\hat{Z}\otimes(\pi/2-\hat{H}_K)} = e^{i\pi\hat{Z}/2} e^{-i\hat{Z}\otimes\hat{H}_K} \tag{40}$$

and

$$(\hat{S}_K)^m = e^{im\pi\hat{Z}/2} e^{-im\hat{Z}\otimes\hat{H}_K}. \tag{41}$$

The select operator can be implemented with just two controlled operators as

$$\hat{S}_K = |0\rangle\langle 0| \otimes \hat{U}_{H_K} + |1\rangle\langle 1| \otimes \hat{U}^{\dagger}_{H_K}. \tag{42}$$

In what follows we choose to implement the $\hat{U}_{H_K}$ using the standard ST decomposition since this decomposition is already known to require adequate resources on the hardware platform [73,74].

A key limitation of the ST formulas in general is that the only operator they can implement is the evolution operator. However, the combination of the arccosine approximation, ST decomposition, and qubitization allows us to approximate polynomials of $\hat{H}$. We will defer a comprehensive generalization of the combined use of these techniques for arbitrary polynomials to future works. For now, utilizing Chebyshev polynomials of the Hamiltonian will suffice in achieving our goal.

From Eq. (41) we see that the Chebyshev moments can be written as

$$T_{2m}(\hat{H}) \simeq (-1)^m \cos(m\hat{H}_K), \quad T_{2m+1}(\hat{H}) \simeq (-1)^m \sin(m\hat{H}_K) \tag{43}$$

that correspond to the real and imaginary part of $e^{im\hat{H}_K}$ up to a sign. Hence, a Hadamard test on top of the random state will correctly implement this operation, as depicted in Fig. 1. Note that, as shown in Fig. 1, a final $\hat{Z}(\eta)$ rotation on the control qubit is needed to implement the component of $\hat{H}_K$ that is proportional to the identity. For $K = 0$ this rotation is simply

$$\hat{Z}(\eta) = e^{i(\mathrm{a}/2\mathrm{b})\hat{Z}}, \tag{44}$$

i.e., $\eta = -\mathrm{a}/\mathrm{b}$, where a and b are defined in Eq. (8). Note that since the random state is used to simulate the maximally mixed state, the circuit of Fig. 1 is a variant of a DQC1.

With such an approximation Eq. (4) translates into

$$D^K_M(E) = \frac{1}{\pi\sqrt{1-E^2}} \Bigg[\gamma^M_0 \mu^K_0 + 2 \sum_{m=1}^{M} \gamma^M_m \mu^K_m T_m(E) \Bigg], \tag{45}$$

where the Chebyshev moments have now been replaced by

$$\mu^K_m = \frac{1}{2^L} \mathrm{Tr}\{\cos[m(\pi/2 - \hat{H}_K)]\}. \tag{46}$$

In the following we will mainly use the first order of this approximation, namely $K = 0$:

$$\mu^0_m = \frac{1}{2^L} \mathrm{Tr}\{\cos[m(\pi/2 - \hat{H})]\}. \tag{47}$$

As discussed at the beginning of Sec. III, to estimate this last quantity, we opted for a DQC1-like circuit, where only one qubit needs to be measured. However, KPM can be extended, as can our method, to estimate other quantities (see Appendix B), where the number of qubits to be measured might increase. In such cases, less naive strategies for applying the final measurement could be beneficial, such as informationally complete measurements [75] or shadow tomography [76]. Finally, it is worth noting that since μ^K_m can be obtained by estimating $\mathrm{Tr}[e^{-im\hat{H}_K}]$, many other protocols could be used in place of the one employed here. In specific cases of the Hamiltonian, the Hadamard test can be simplified by avoiding the application of the controlled operator, as shown in Ref. [77]. An alternative to the Hadamard test is the Loschmidt echo test [78], which has also been used to compute the real and imaginary part of unitary operators. Several other approaches to this problem can also be found in [26], where qudits and analog devices are also taken into account.

Computing many-body statistical properties appears as something NISQ devices are already able to afford. A comparison with other proposals to do it is presented in Appendix C where in particular we show the close similarity of our method with the one presented in Ref. [26].

IV. RESULTS ON THE QUANTINUUM H1-1 DEVICE

A. Example model to be simulated

As a test model to implement our algorithm on quantum hardware we choose the nonintegrable spin-$\frac{1}{2}$ XYZ Heisenberg chain with a staggered interaction along the Z direction:

$$\hat{H} = \sum_{i=0}^{L-1} J_x \hat{X}_{(i)}\hat{X}_{(i+1)} + J_y \hat{Y}_{(i)}\hat{Y}_{(i+1)} + J_z \hat{Z}_{(i)}\hat{Z}_{(i+1)} + \sum_{i=0}^{L-1} (-1)^i \Lambda \hat{Z}_{(i)}\hat{Z}_{(i+1)}. \tag{48}$$

By choosing $J_z = \Lambda$, we can add a small advantage from the perspective of gate count, without adding any symmetry to the Hamiltonian. Indeed, the exponentiation of $\hat{H}$ [Eq. (48)] can be split into two noncommuting terms: interactions between even-odd spins and between odd-even spins. The latter, when $\Lambda = J_z$, have nonzero couplings only along the X and Y direction. Then, even-odd terms require a gate composition of Fig. 6(b), while odd-even terms require the even shallower Fig. 6(a). The nonintegrability of this Hamiltonian arises from the staggered interaction along the z axis, as discussed in Ref. [79]. The absence of conserved quantities within these systems not only renders computational tasks more challenging but also prevents the emergence of specific patterns in the energy distribution. Consequently, the system exhibits a faster convergence toward a Gaussian-like shape. This latter behavior, which directly stems from the central limit theorem, is a well-established characteristic observed in various physical

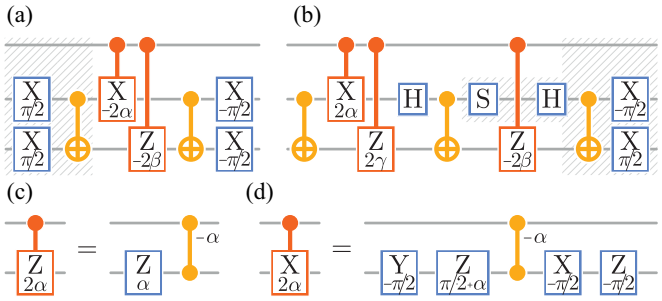

FIG. 6. Gate decompositions used to implement the controlled unitary (i.e., the orange gate of Fig. 1) for the Hamiltonian of Eq. (48). The controlled ST decomposition of this Hamiltonian requires a controlled $\exp(i\alpha\hat{X}\otimes\hat{X}+i\beta\hat{Y}\otimes\hat{Y})$ for the odd-even spin pairs (a) and a controlled $\exp(i\alpha\hat{X}\otimes\hat{X}+i\beta\hat{Y}\otimes\hat{Y}+i\gamma\hat{Z}\otimes\hat{Z})$ for the even-odd spin pairs (b), with $\alpha,\beta,\gamma\in\mathbb{C}$. The hatched area in (a) represents the part that for the first ST step will naturally mix with the last layer of the random circuit, without requiring additional gates; the hatched area of (b) in the last ST step can be neglected. Panels (c) and (d) respectively represent the conversion of the C-$\hat{Z}(2\alpha)$ and C-$\hat{X}(2\alpha)$ in the native gate set currently supported by the system model H1-1. Note that this particular gate decomposition was chosen in order to require as few gates as possible on the control qubit, to enhance parallelization and reduce the probability of errors occurring.

systems, such as lattices of interacting quantum systems in arbitrary dimensions and arbitrary interactions [80].

B. Hardware results

We are now in a position to test our quantum algorithm on physical hardware using the model described above. To evaluate the effectiveness of the method at each stage of approximation, we conducted quantum and classical simulations of the chain defined by Eq. (48) at $L=12$ and $L=18$. In Fig. 7, we compare the Chebyshev moments obtained by various methods: by analytical calculation (using eigenvalues obtained from ED), by approximating the arccos function, by including the ST approximation, and by simulating the circuit of Fig. 1 with and without noise. To generate the random state, we implemented a series of gates on the L-qubit register via the Par. method, as described in Sec. III A. The Chebyshev moments were computed using the methods described in Sec. III B, taking the arccosine expansion to order $K=0$, i.e., $\arccos(\hat{H})\approx\pi/2-\hat{H}$, and using a single ST step. Remarkably, we find that even with these parameters it is possible to achieve an appreciable precision. We found that hardware errors overcome any attainable improvements from using arccosine expansions with $K>0$ or more than a single ST step. More detail on the error analysis is given in Appendix D.

We found that for $L=12$, the KPM expansion reaches a sufficient degree of convergence to ED values at $M\sim 25$. Due to resource limitations on the Quantinuum device we used only four different random states, running 1000 shots for each one of these. We simulated up to $m=7$ on the quantum hardware, and approximate $\mu_m\approx 0$ for $m>7$, since these moments are too small to be distinguished from zero with

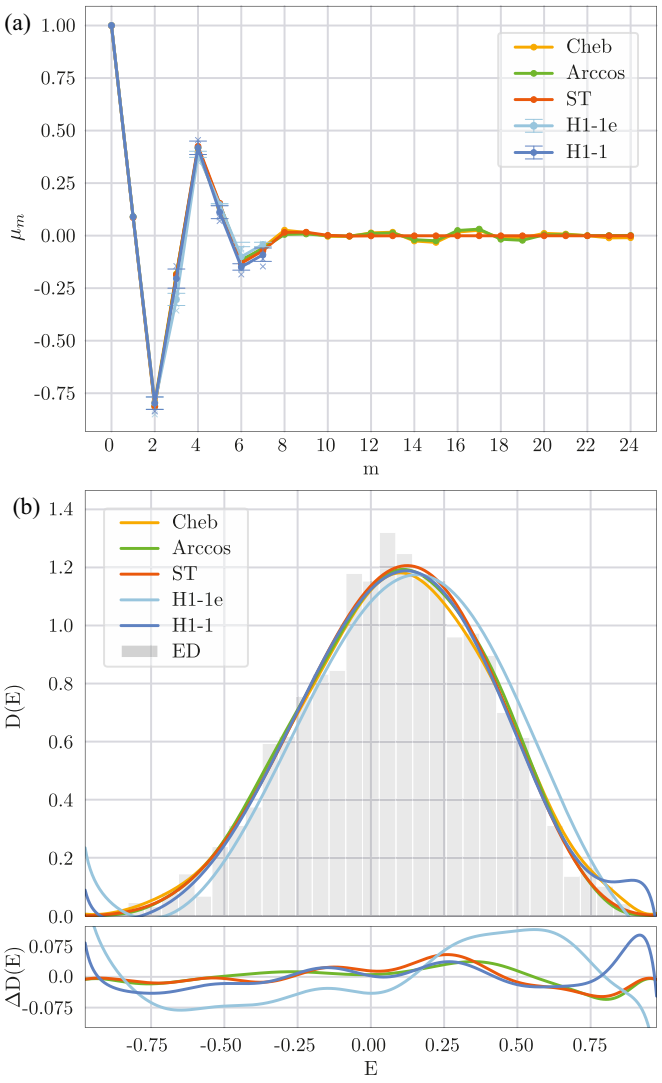

FIG. 7. Results for the Hamiltonian of Eq. (48) at $L=12$ with $J_x=1, J_y=1/3, J_z=\Lambda=1/2$. In (a) the estimates for the first 25 Chebyshev moments. The comparison is between Chebyshev moments obtained in different ways: analytically (Cheb), applying the arc-cosine approximation at the first order (Arccos), adding the ST approximation with one single step (ST), and the results from the circuit of Fig. 1 from Quantinuum, the emulator (H1-1e) and the quantum computer (H1-1). We used 4 different random circuits ($R=4$) with $j=5$ and 1000 shots. Each cross represents the result from a circuit with a different random circuit. Panel (b) is composed by two parts. On top: the DOS obtained with the five different estimates for the Chebyshev moments (using a kernel with $M=25$) and the DOS from the exact diagonalization (ED). On bottom we reported the comparison of the DOS obtained with different approximation of the Chebyshev moments with respect to the analytical ones.

our resources (see Appendix D). Figure 7(b) shows that the moments extracted from the quantum computer are almost indistinguishable from the exact values within the bulk of the spectrum, and that the KPM with $M=25$ is able to accurately reconstruct the DOS using these moments.

We next attempted the same calculation on a register of $L=18$, which uses 19 out of 20 qubits currently available on the H1-1 system [37]. Here the KPM requires $M\sim 50$

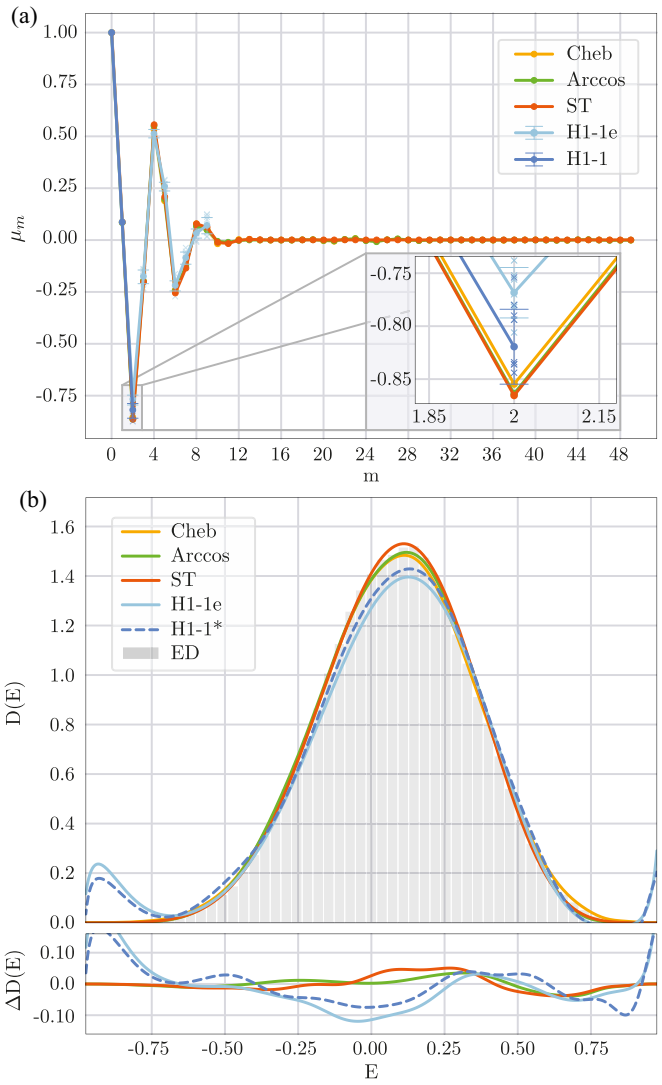

FIG. 8. Similarly to Fig. 7, the results for the Hamiltonian of Eq. (48) at $L = 18$ with $J_x = 1, J_y = 1/3, J_z = \Lambda = 1/2$. In (a) the estimates for the first 50 Chebyshev moments. Here, for the Quantinuum executions, we used 10 different random circuits ($R = 10$) with $j = 4$ and 1000 shots. Each cross represents the result from a circuit with a different random circuit. Panel (b) is composed by two parts. On top: the DOS obtained with the five different estimates for the Chebyshev moments and the DOS from the exact diagonalization (ED). Since we computed μ_2 only from the H1-1 system, we also included what the DOS estimate from the μ_2 from the real hardware combined with the estimates from the emulator would look like (H1-1*). On bottom we reported the comparison of the DOS obtained with different approximation of the Chebyshev moments with respect to the analytical ones.

to achieve an accurate approximation, while the moments that can be simulated accurately range up to $m = 11$, beyond which their values become too small to be distinguished from zero given the number of shots we have used. Simulating a larger system requires even more resources, and due to the higher costs associated with these larger circuits, we ultimately only simulated μ_2 on the real hardware for the $L = 18$ case as it can be observed in the inset of Fig. 8(a). Our results demonstrate that the emulator (H1-1e) consistently produces accurate outcomes and we compute the rest of the moments with it. Additionally, we note that the fidelity of the $\hat{Z}\hat{Z}$ gate appears to improve with smaller angles. Our circuit heavily employs these gates (see Fig. 6), and any discrepancies in the emulator results can be attributed to an underestimation of these gates' fidelities. We report the results from this last system in Fig. 8, where in the plot of the DOS we add a projection obtained by combining the results from hardware and emulator together. Finally, it is worth noting that all the results presented herein have been obtained without employing error mitigation techniques. This observation demonstrates the favorable performance of the algorithm on Quantinuum's hardware, while also facilitating the reproducibility of our results and the scalability of our techniques.

V. CONCLUSIONS

In summary, we have performed an estimation of the density of states of a nonintegrable many-body quantum system on a digital quantum simulator. We have designed and implemented a quantum algorithm that approximates the Chebyshev moments as the amplitude of the evolution operator of $\hat{H}_K$ which for $K = 0$ is just the Hamiltonian. In particular we extract them through a combination of the Hadamard test, Suzuki-Trotter decomposition, and random-state preparation. Proof-of-principle hardware simulations were performed on registers of $L = 12$ and $L = 18$ qubits on the Quantinuum H1-1 ion trap quantum computer, obtaining a good approximation to the DOS for a nonintegrable Hamiltonian in the bulk of the spectrum (corresponding to high microcanonical temperatures). We explored in detail the crucial subroutines of stochastic trace evaluation and controlled evolution with arccosine approximation. We believe that our quantum hardware results represent the current state of the art, in terms of both the generation of pseudorandom states and the implementation of controlled unitary operations on a many-qubit register. We emphasise that the accuracy of our hardware results has been limited primarily by financial constraints, and not by fundamental resource scalings or even by noise on the H1-1 device.

For the DOS we found it was sufficient to take the arccosine expansion to very low order ($K = 0$), which is ultimately due to the concentration of energy levels at the center of the spectrum in large systems. We note that our KPM-inspired approach can easily be tailored to compute finite-temperature expectation values in the diagonal and microcanonical ensembles, in addition to other spectral functions such as the Lehmann representation of multitime correlation functions. In these cases, it may be necessary to consider higher-order expansions (i.e., $K > 0$) to account for features away from the center of the spectrum. Our methods could also be combined with other quantum algorithms tailored to compute ground-state and low-lying excited state properties [16–21], in order to estimate thermodynamic properties across the full range of temperature scales.

Our estimation of the DOS on current quantum hardware represents an important step forward toward quantum statistical mechanics calculations on quantum computers. As the devices improve, we expect that this algorithm and

subroutines can be used to extract useful approximations to thermodynamic properties in regimes not accessible to state-of-the-art classical numerical techniques for strongly correlated systems.

ACKNOWLEDGMENTS

J.G. would like to thank Sabrina Maniscalco for inviting him to take part in an unconference in Lapland where some of the first discussions related to this work took place. We thank Microsoft Ireland, in particular Kieran McCorry, for providing generous funding to run this project and for providing access to the Quantinuum machine through Microsoft Azure Quantum. A.S. would like to express thanks to both the QuSys and ToCQS groups for their consistent feedback and valuable suggestions. J.G. is supported by a SFI–Royal Society University Research Fellowship. J.G. and C.C. acknowledge funding from European Research Council Starting Grant ODYSSEY (Grant Agreement No. 758403). M.T.M. is supported by a Royal Society–Science Foundation Ireland University Research Fellowship (No. URF/R1/221571).

APPENDIX A: DECONSTRUCTING THE KEY COMPONENTS OF KPM

Given a function f, a family of orthogonal functions $\{g_M\}$ such that

$$f(x) \approx g_M(x) = \sum_{m=0}^{M} a_m \Phi_m(x) \tag{A1}$$

is said to be a good approximation if it approximates f in at least the square norm:

$$\|f(x) - g_M(x)\|_2 = \left[\int [f(x) - g_M(x)]^2 dx\right]^{1/2}. \tag{A2}$$

A family of functions that are frequently used for this scope is given by Fourier series. In this case, the polynomials are

$$g_M(x) = \frac{1}{2}a_0 + \sum_{m=1}^{M} [a_m \cos(mx) + b_m \sin(mx)] \tag{A3}$$

where the coefficients are

$$a_m = \frac{1}{\pi}\int f(x)\cos(mx)dx,$$
$$b_m = \frac{1}{\pi}\int f(x)\sin(mx)dx. \tag{A4}$$

The Fourier decomposition works well with signals, namely with processes that happen to be periodic and extended in time (its convergence domain is an infinite strip, symmetric around the real axes [81]). Similarly, we can evaluate f (and the coefficients a_m and b_m) just in the $[-\pi, \pi]$ interval. The Fourier series is then exponentially convergent for periodic functions with derivatives bounded in $[-\pi, \pi]$; namely its coefficients a_m and b_m decrease exponentially in m:

$$a_m, b_m \sim O[\exp(-qn^r)] \tag{A5}$$

with $n \gg 1$ and q a constant for some $r > 0$. If f is even (odd) all the sine (cosine) coefficients will cancel out and the expansion becomes the *Fourier sine (cosine) series*.

Many physical phenomena are not periodic but bounded (occur in a limited space). Since the Fourier series properly works with periodic functions only, one can apply a change of variable

$$x = \cos(\theta)$$

with then $\theta \in [-\pi, \pi] \to x \in [-1, 1]$. This change of variable transforms the function to a periodic one, allowing for the application of the Fourier series. Noticing that $f(\cos(\theta)) = f(\cos(-\theta))$ the expansion reduces to the Fourier cosine series:

$$g_M(\cos(\theta)) = \sum_{m=0}^{M} a_m \cos[m\cos(\theta)], \tag{A6}$$

where $\cos[m\cos(\theta)]$ are the Chebyshev polynomials $T_m(\cos(\theta))$. Reformulating this last equation in x we have

$$g_M(x) = \frac{1}{\pi\sqrt{1-x^2}} \sum_{m=0}^{M} a_m T_m(x), \tag{A7}$$

where now

$$T_m(x) = \cos[m \arccos(x)] \tag{A8}$$

and we added the coefficient $1/(\pi\sqrt{1-x^2})$, which serves as the weight for the orthogonality of these polynomials. Due to this strong connection with the Fourier series, the Chebyshev series inherits all its properties (among which the exponential convergence) with now the advantage to be working also with nonperiodic functions.

We can notice that $\cos[m \arccos(x)]$ is actually a polynomial in x by looking at the identity

$$\cos(2\phi) = \cos^2(\phi) - 1 \tag{A9}$$

which leads to the following iterative property of the Chebyshev polynomials:

$$T_0(x) = 1,$$
$$T_1(x) = x,$$
$$T_{m+1}(x) = 2xT_m(x) - T_{m-1}(x). \tag{A10}$$

The Chebyshev expansion, as established in Ref. [82], stands out as the optimal expansion technique for continuous functions. Nevertheless, when truncated, it engenders the emergence of Gibbs oscillation effects. To effectively mitigate these effects, one can convolve the expansion presented in Eq. (A12) with a kernel function. Among the available options, the Jackson kernel, which is also our chosen approach, stands as the most widely adopted solution,

$$\gamma_m^M = \frac{(M-m+1)\cos\frac{\pi m}{M+1} + \sin\frac{\pi m}{M+1}\cot\frac{\pi}{M+1}}{M+1}, \tag{A11}$$

yielding to

$$g_M(x) = \frac{1}{\pi\sqrt{1-x^2}} \sum_{m=0}^{M} \gamma_m^M a_m T_m(x), \tag{A12}$$

where this last expression correctly converges to the original one:

$$\|f - g_M\|_\infty \sim O(1/M). \tag{A13}$$

A detailed derivation of the Jackson kernel can be found in Ref. [28].

APPENDIX B: ESTIMATING QUANTUM THERMAL AVERAGES

While our method was initially benchmarked on the DOS, the quantum subroutine can be readily adapted for the broader purpose of estimating Chebyshev moments with respect to an observable $\hat{A}$:

$$\mu_{m,A} = \mathrm{Tr}[\hat{A}T_m(\hat{H})], \tag{B1}$$

and similarly for the arccosine approximated ones:

$$\mu^K_{m,A} = \mathrm{Tr}[\hat{A}\cos(m(\pi/2 - \hat{H}_K))]. \tag{B2}$$

This adaptation allows us to construct the spectral function $A_M(E)$ using the KPM as

$$A_M(E) = \frac{1}{\pi\sqrt{1-E^2}}\left[\gamma_0^M\mu_0 + 2\sum_{m=1}^{M}\gamma_m^M\mu_{m,A}T_m(E)\right], \tag{B3}$$

where in the arccosine-approximated version $A^K_M(E)$, the moments $\mu_{m,A}$ are replaced by the approximated ones $\mu^K_{m,A}$.

Thus, one can compute the canonical observables estimate at finite temperature as

$$A(\beta) = \frac{\mathrm{Tr}[\hat{A}e^{-\beta\hat{H}}]}{\mathrm{Tr}[e^{-\beta\hat{H}}]} = \frac{\int e^{-\beta E}A_M(E)dE}{\int e^{-\beta E}D_M(E)dE}. \tag{B4}$$

To modify the circuit of Fig. 1, there are two options: inserting an operator $\hat{M}_A$, where $\hat{A} = \hat{M}_A^\dagger\hat{M}_A$, between the random circuit and the controlled unitary, or performing a basis change after the controlled unitary and measuring the qubits on which $\hat{A}$ operates on [34]. The first approach necessitates ancillary qubits to implement the nonunitary operator $\hat{M}_A$, while the latter requires measuring additional qubits in the L-qubit register.

To explore a specific segment of the spectrum, $[\eta' - \Delta, \eta' + \Delta]$, one can introduce a Hamiltonian shift, represented as $d\eta = \eta' - \eta$, and then exclusively integrate Eq. (B3) within this interval. In this case the Chebyshev polynomials will become

$$\mu^{K(d\eta)}_{m,A} = \mathrm{Tr}[\hat{A}\cos(m(\pi/2 - \hat{H}_K - d\eta))]. \tag{B5}$$

In Fig. 9(a) we reconstructed the DOS of a spin chain with $L = 12$ while in Fig. 9(b) we report the results for the spectral distribution of the observable $\hat{A} = \hat{Z}_0\hat{Z}_1$ (see also Fig. 10). We split the spectrum in seven parts with the same width and finally we estimate the thermal average of $\hat{Z}_0\hat{Z}_1(\beta)$.

APPENDIX C: COMPARISON WITH OTHER METHODS

Based on Appendix B, the proposed methodology can be effectively applied to estimate the statistical properties of a quantum system. The computation of these properties on quantum devices has witnessed significant advancements. These advancements have predominantly focused on estimating observables through two primary strategies where the observables are estimated either on a direct construction of thermal states [83,84] or on an evolved ensembles of pure states [23,25,26,85]. Constructing thermal states still presents several challenges [86] and with a keen eye on the practical constraints imposed by NISQ devices, two methodologies using the latter strategy stand out: the cosine filter of Ref. [26] and QMETTS, discussed in Refs. [25,87].

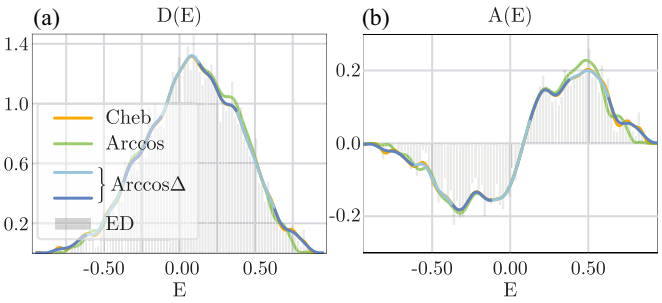

FIG. 9. (a) Estimations of the density of states (DOS) and (b) spectral distribution of the observable $\hat{A} = \hat{Z}_0\hat{Z}_1$ were conducted using ED along with various executions of the KPM. The Hamiltonian employed is identical to the one depicted in Fig. 7 ($L = 12$), and in this case, we used $M = 75$. In yellow (Cheb) the results obtained by using the exact Chebyshev polynomials (μ_m and $\mu_{m,A}$); in green (Arccos) the ones from the first approximation of the arccosine approximation (μ^0_m and $\mu^0_{m,A}$). Furthermore, we employed a KPM approach to compute moments within seven distinct intervals, each highlighted alternately in blue and light blue. These intervals correspond to varying values of $d\eta$, specifically $d\eta = 0, \pm0.25, \pm0.5, \pm0.75$. The computed moments, denoted as $\mu^{0(d\eta)}_{m,A}$, were considered only within a range of $\pm\Delta$ around the corresponding $d\eta$ values.

The former method [26] relies upon the utilization of the cosine-filtering operator in lieu of the Hamiltonian to suppress eigenvectors lying beyond a predefined energy spectral window. This operator is defined as

$$P_\delta = \left[\cos\left(\frac{\hat{H} - E}{L}\right)\right]^{\lfloor L^2/\delta^2\rfloor_2}, \tag{C1}$$

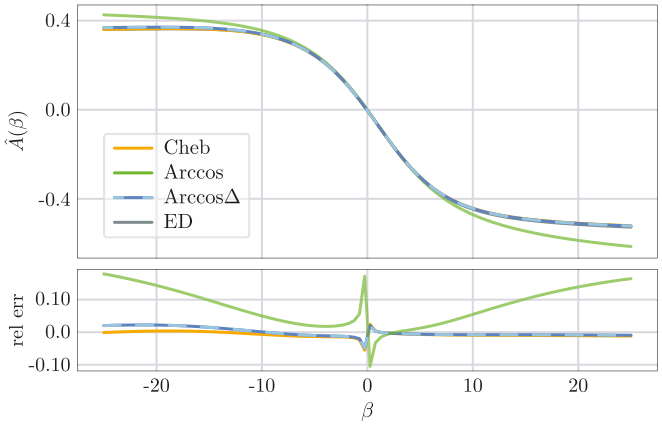

FIG. 10. Calculation of the canonical average for $\hat{A} = \hat{Z}_0\hat{Z}_1$ is achieved through the utilization of spectral functions acquired from Fig. 9. The lower portion of the figure presents the relative error in comparison to values obtained through ED. Integration is performed over the energy range encompassing $[-0.75, 0.75]$.

where $\lfloor\cdot\rfloor_2$ indicates the nearest even integer and δ is either a constant or a factor scaling poly$(1/L)$. In the following we will indicate $\lfloor L^2/\delta^2\rfloor_2$ as M. By using this operator canonical observables are been estimated by measuring on the quantum computer only quantities of the form

$$a_\psi(t) = \langle\psi|\, e^{-it\hat{H}}\,|\psi\rangle\,,$$
$$a_{\psi,A}(t) = \langle\psi|\,\hat{A}e^{-it\hat{H}}\,|\psi\rangle\,. \tag{C2}$$

For example the DOS can now be approximated as

$$D_{\delta,\psi}(E) = \frac{1}{2^M}\sum_{m=-x\sqrt{M}}^{x\sqrt{M}}\binom{M}{\frac{M}{2}-m}e^{-i\frac{2m}{L}(E-E_\psi)}a_\psi(2m/L), \tag{C3}$$

where the cosine filter operator of Eq. (C1) is approximated with an error dominated by $2e^{-x^2/2}$, where therefore the coefficient x controls this error.

Eventually, to estimate canonical observables, the final expression of the cosine-filter method is

$$A_\delta(\beta) = \frac{\int dE e^{-\beta E}\int d\mu_\psi A_{\delta,\psi}(E)}{\int dE e^{-\beta E}\int d\mu_\psi D_{\delta,\psi}(E)}, \tag{C4}$$

where $A_{\delta,\psi}$ is obtained by replacing $a_\psi(2m/L)$ with $a_{\psi,A}(2m/L)$ in Eq. (C3), adding its complex conjugate and dividing everything by two.

Estimating $a_\psi(t)$ $[a_{\psi,A}(t)]$ corresponds to being able to estimate $\langle\psi|\cos(2m\hat{H}/L)\,|\psi\rangle$ $[\langle\psi|\,\hat{A}\cos(2m\hat{H}/L)\,|\psi\rangle]$ and vice versa. To bridge the gap between the cosine-filter method and ours we can start by splitting the spectrum in intervals, as done in the previous section. As the width of the intervals approaches zero, they increase in number, and the rearranged expansion of the local KPM will make no use of Chebyshev polynomials:

$$D^0_M(E) = \frac{1}{\pi}\sum_{m=-M}^{M}\gamma^M_{|m|}e^{im\pi/2}e^{i\frac{m}{\mathrm{b}}E}a_I(m/\mathrm{b}), \tag{C5}$$

where we considered the non-normalized Hamiltonian [i.e., before the mapping of Eq. (8)] as in the cosine-filter method and we defined $a_I(m) = \mathrm{Tr}[e^{-im\hat{H}}]$. Note that no sign problem is caused by $e^{im\pi/2}$ as it only selects real or imaginary parts of $a_I(m/\mathrm{b})$. Furthermore, we can notice that the coefficients of Eq. (C5) are $\leqslant 1/\pi$ while the ones of Eq. (C3) are $\leqslant \sqrt{2/(\pi M)}$.

Therefore, the analog expression to Eq. (C4) reads

$$A(\beta) = \frac{\int dE e^{-\beta E}A_M(E)}{\int dE e^{-\beta E}D_M(E)}. \tag{C6}$$

The most notable distinction between Eq. (C4) and Eq. (C6) is the absence of integration over the states ψ as we only need to compute the trace of the evolution operator. According to Eq. (A13), the maximum time required to achieve an error of $O(1/M)$ is M/b, where b scales with the system size.

In contrast, in Ref. [26], for a fixed error, the maximum time is $2x/\delta$. As mentioned earlier, x determines the approximation to the original cosine-filter operator, while δ is either a constant or scales maximally as poly$(1/L)$ (depending on the system). This results in the maximum time being independent of the system size or scaling as $\sim$poly(L).

The latter method instead, QMETTS, is based on the METTS algorithm [88] which is a sampling method to calculate thermal properties based on imaginary time evolution. Equation (B4) is so rephrased as

$$A(\beta) \simeq \frac{\sum_i \|\psi_i\|^2\,\langle\psi_i|\,\hat{A}\,|\psi_i\rangle}{\sum_i\|\psi_i\|} = \sum_i p_i\,\langle\psi_i|\,\hat{A}\,|\psi_i\rangle\,, \tag{C7}$$

where $|\psi_i\rangle = e^{-\beta\hat{H}}\,|\phi_i\rangle$ and ϕ_i are a randomly sampled set of low-entanglement states, which in Refs. [25,87] are product states. QMETTS is proposed to be the quantum version of METTS and it is based on the QITE routine. In this routine an initial state is evolved by an imaginary time by finding the analog real time operator. Beginning with the ϕ_i states, QMETTS leverages QITE to evolve these states before evaluating the observable on them. As such, this last method also relies on the quantum device's ability to estimate the amplitude of an evolution operator. A key distinction of QMETTS, which complicates a direct comparison with ours and the cosine-filter method is that the temperature of the thermal average β corresponds to the imaginary time the initial states ϕ_i have to be evolved to. In contrast, the other techniques, which operate through the energy spectrum, provide an initial estimate of the thermal average for any temperature.

APPENDIX D: ERROR ANALYSIS

Our method builds upon the standard KPM by employing a quantum computer to store the Hamiltonian and compute an approximation of the Chebyshev moments. This renders it an approximation of the standard KPM, which then can be used as a benchmark for evaluating the accuracy of our approach. As previously described, the KPM converges uniformly as $O(1/M)$, where M is the order of maximum Chebyshev moment. In our method, we simplify the Chebyshev moments by approximating the arccosine function. To study the specific scaling of this approximation, we will once again examine the non-normalized Hamiltonian, $(\hat{H}-\mathrm{a})/\mathrm{b}$, as discussed in the previous section. The error associated with this approximation depends on the distribution of the Hamiltonian's eigenvalues. For odd terms we have

$$\left|\mathrm{Tr}\left[T^K_{2M+1} - T_{2M+1}\right]\right| \sim \left|\mathrm{Tr}[(2M+1)^2(\hat{H}/\mathrm{b})^{2K+4}]\right|, \tag{D1}$$

where $T^K_M(x) = \cos[M(\pi/2 - \sum_{k=0}^K c_k x^{2k+1})]$, and similarly for evens

$$\left|\mathrm{Tr}\left[T^K_{2M} - T_{2M}\right]\right| \sim O(|\mathrm{Tr}[(2M)^2(\hat{H}/\mathrm{b})^{2K+3}]|). \tag{D2}$$

Therefore, the overall error in the DOS will go as

$$\left|D^K_M(E) - D_M(E)\right| \sim O(M^2/L^{K+1.5}), \tag{D3}$$

where we assumed again that $\mathrm{b}\sim L$. From this last equation we can observe that by increasing the order of the Chebyshev expansion (M), the error will increase. Additionally, notice that the error in Eq. (D3) depends on the ratio $\sim(\hat{H}/L)^{2K+3}$. The variance of the DOS only scales as L, which yields to a final scaling of $\sim L^{-(K+1.5)}$. This scaling of the variance of the DOS can be observed by connecting this quantity with an extensive quantity, as the heat capacity. In fact, by assuming the DOS to be roughly a Gaussian,

the entropy will be $S(E) = \ln D(E) \sim -(E - E_I)^2/(2\sigma_I^2)$. Therefore,

$$C = -\beta^2 \left(\frac{d^2 S(E)}{dE^2} \right)^{-1} = \beta^2 \sigma_I^2, \tag{D4}$$

from which we can see that $\sigma_I \sim \sqrt{C} \sim \sqrt{L}$. While the KPM error and this last from the arccosine approximation are intrinsic errors of our method, the full digitalization still requires two further approximations. Implementing the evolution operator on a circuit is a well studied problem. Using the Quantinuum device puts the constraint of minimizing the number of different circuits, which made us choose the standard ST approximation. Otherwise a better scaling can be achieved with qDrift [63], with the advantage of having to implement as complex operators as with the ST approximation. As the coefficients c_k decrease exponentially with respect to k, and since higher powers of coefficients of a normalized Hamiltonian also rapidly decrease, the evolution of $\hat{H}_K$ appears to be particularly well suited for this method. Finally, stochastic trace estimation introduces an error that decreases exponentially with L: $O(1/\sqrt{R2^L})$. However, as noted at the end of Sec. III A, this error is still dominated by shot noise, except when routines like amplitude amplification are included. Therefore, pseudorandom states can be replaced with random bit strings. The final error due to shot noise scales as $O(1/\sqrt{\text{shots}})$.

APPENDIX E: HIGHER ORDERS OF THE ARCCOSINE EXPANSION

As shown in Fig. 7(b) and Fig. 8(b), due to the concentration of eigenstates around zero, for a lot of physical Hamiltonians the first-order expansion is enough to approximate the DOS. In case a better precision is required, one can truncate the arccos approximation to the second order (i.e., $K = 1$). At this order of approximation, a k-local Hamiltonian would become $3k$-local. However, the terms that are actually $3k$-local contribute to a lesser degree. Moreover, a large part of $\hat{H}^3$ will lie on the same operators of $\hat{H}$. For instance, in the Hamiltonian of Eq. (48) the only coefficients in $\hat{H}^3$ that increase with the system size are the ones of Pauli operators already present in $\hat{H}$. Indeed, one can simply implement the same combination of Pauli operators of $\hat{H}$ by *updating* the parameters to include the contributions from $\hat{H}^3/6$. Considering the case $J_z + \Lambda = J_x$ in Eq. (48), the coefficient of the terms $\hat{X}_{(i)}\hat{X}_{(i+1)}$ coupling even to odd sites is updated from J_x to

$$J_x\left\{1 + \tfrac{1}{6}\left[(9L/2 - 2)J_x^2 + (3L - 4)J_y^2 + 3\beta^2 + 6J_y\beta\right]\right\}, \tag{E1}$$

while the coefficient of the odd to even terms is updated from J_x to

$$J_x\left\{1 + \tfrac{1}{6}\left[(9L/2 - 6)J_x^2 + (3L - 4)J_y^2 + 3\beta^2\right]\right\}. \tag{E2}$$

Similarly, the J_y for the terms $\hat{Y}_{(i)}\hat{Y}_{(i+1)}$ coupling even to odd sites is modified to

$$J_y + \tfrac{1}{6}\left[(3L - 2)J_y^3 + (9L/2 - 4)J_yJ_x^2 + 3J_y\beta^2 + 6J_x^2\beta\right], \tag{E3}$$

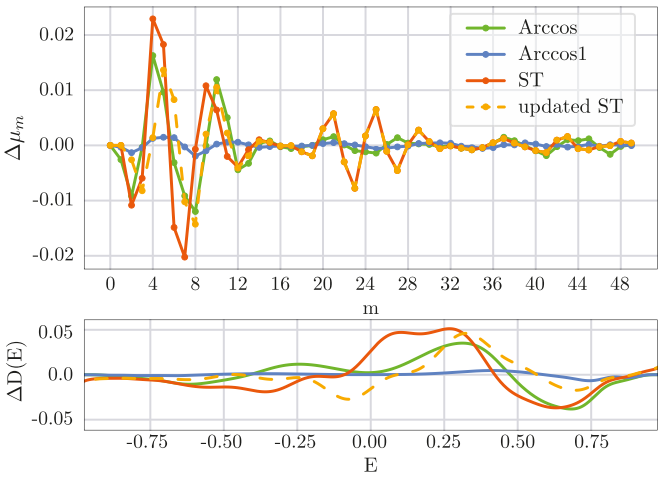

FIG. 11. Comparison of the first 50 analytical Chebyshev moments with different approximations: the first-order arccosine approximation (Arccos); the second, which involves the 3rd power of the Hamiltonian (Arccos1); the normal ST approximation at the first order (ST) and its version with the updated parameters (updated ST). After $m = 15$ the difference between these last two approximations becomes negligible.

and J_y of the odd-even ones to

$$J_y\left\{1 + \tfrac{1}{6}\left[(3L - 2)J_y^2 + (9L/2 - 8)J_x^2 + 3\beta^2\right]\right\}. \tag{E4}$$

As for the z coupling, our Hamiltonian only has even terms where the coefficient is updated as

$$J_x\left\{1 + \tfrac{1}{6}\left[(9L/2 - 6)J_x^2 + (3L - 4)J_y^2 + 3\beta^2 + 6J_y\beta\right]\right\}, \tag{E5}$$

and, finally, the coefficient of the identity becomes

$$\beta + \tfrac{1}{6}\left(-\beta^3 - 3LJ_y^2 - 9/2L\beta J_x^2 - 3LJ_x^2J_y\right). \tag{E6}$$

The comparison of how the ST decomposition is affected by using these parameters instead of the initial ones is reported in Fig. 11.

APPENDIX F: POWERS OF THE HAMILTONIAN

In this Appendix, we review how a similar approach to the arccosine approximation can be adapted to implement the powers of the Hamiltonian. In Ref. [89], Seki and Yunoki devise a method to implement powers of a Hamiltonian as the finite time derivative of the evolution operator, based on the idea that

$$\hat{H}^m = i^m \frac{d^m \hat{U}(t)}{dt^m}\bigg|_{t=0}. \tag{F1}$$

At a finite time t, the authors suggest taking the central derivative and for the first power of the Hamiltonian the equation becomes

$$\hat{H} \simeq \frac{i}{2t}(e^{-it\hat{H}} - e^{it\hat{H}}). \tag{F2}$$

This is equivalent to approximating the Hamiltonian as

$$\hat{H} \simeq \frac{e^{it\hat{H}} - e^{-it\hat{H}}}{2it} = \frac{\sin(t\hat{H})}{t}. \tag{F3}$$

A closer look reveals that the first-order approximation of the sine corresponds to the first-order approximation of the arcsine in

$$\hat{H} = \frac{e^{i \arcsin t\hat{H}} - e^{-i \arcsin t\hat{H}}}{2it} \simeq \frac{1}{2it}(e^{i(t\hat{H})_K} - e^{-i(t\hat{H})_K}), \tag{F4}$$

namely, an alternative two-unitary decomposition to the one of Eq. (29) with the arcsine instead of the arccosine in Eq. (30). This offers a path to increasing the precision of the method in a more controlled way. Furthermore, the coefficients of the expansion can be tailored so that the powers of $\hat{H}$ in the expansion will elide together:

$$c_k = -\frac{(-1)^k}{(2k+1)!} - \frac{(-1)^{k'}(c_{k'})^{2k'+1}}{(2k'+1)!} \tag{F5}$$

if $\exists\, k' \in \mathbb{N}$ such that $2k'+1 = \sqrt{2k+1}$, and

$$c_k = -\frac{(-1)^k}{(2k+1)!} - \frac{(-1)^{n'} c_{k'}^{2n'+1}}{(2n'+1)!} - \frac{(-1)^{k'} c_{n'}^{2k'+1}}{(2k'+1)!} \tag{F6}$$

if $\exists\, k', n' \in \mathbb{N}, k' \neq n'$ such that $2k+1 = (2k'+1)(2n'+1)$, and otherwise

$$c_k = -\frac{(-1)^k}{(2k+1)!}. \tag{F7}$$

In this way the error will scale as $O[(t\hat{H})^{2K+1}]$.

As highlighted, the probability of successfully selecting the combination of unitaries will depend on the magnitude of the trace of the product of t and $\hat{H}$. Therefore, if the Hamiltonian has a large trace, as

$$\hat{H} = J \sum_i \hat{I} + \hat{X}_{(i)}\hat{X}_{(i+1)} + \hat{Y}_{(i)}\hat{Y}_{(i+1)} + \hat{Z}_{(i)}\hat{Z}_{(i+1)}, \tag{F8}$$

it will be possible to take small time steps and still have a non-negligible trace. Otherwise, if the Hamiltonian is normalized it will be necessary to take $t \lesssim 1$.

Alternatively, since by including higher orders of the arccosine approximation the less local terms will have small coefficient, the effective Hamiltonian will be suited for approaches like qDrift [63], where the unitary operator can be controlled as described in [90]. In these procedures the deterministic compiler is replaced by a stochastic one where the operators employed in the standard Suzuki-Trotter decomposition are picked randomly, with a probability that depends on their coefficient. This protocol allows a simpler numerical analysis. If the Hamiltonian is decomposed as

$$\hat{H} = \sum_{p=0}^{P} h_p \hat{H}_p \tag{F9}$$

the depth of the circuits required by qDrift will depend on the sum of the h_p coefficients, rather than just the largest coefficient and P, as is the case for the standard Suzuki-Trotter decomposition.

[1] R. P. Feynman, Simulating physics with computers, Int. J. Theor. Phys. **21**, 467 (1982).

[2] S. Lloyd, Universal quantum simulators, Science **273**, 1073 (1996).

[3] I. M. Georgescu, S. Ashhab, and F. Nori, Quantum simulation, Rev. Mod. Phys. **86**, 153 (2014).

[4] F. Tacchino, A. Chiesa, S. Carretta, and D. Gerace, Quantum computers as universal quantum simulators: State-of-the-art and perspectives, Adv. Quantum Technol. **3**, 1900052 (2020).

[5] A. J. Daley, I. Bloch, C. Kokail, S. Flannigan, N. Pearson, M. Troyer, and P. Zoller, Practical quantum advantage in quantum simulation, Nature (London) **607**, 667 (2022).

[6] J. Preskill, Quantum computing in the NISQ era and beyond, Quantum **2**, 79 (2018).

[7] A. A. Zhukov, S. V. Remizov, W. V. Pogosov, and Y. E. Lozovik, Algorithmic simulation of far-from-equilibrium dynamics using quantum computer, Quantum Inf. Process. **17**, 223 (2018).

[8] A. Cervera-Lierta, Exact Ising model simulation on a quantum computer, Quantum **2**, 114 (2018).

[9] A. Francis, J. K. Freericks, and A. F. Kemper, Quantum computation of magnon spectra, Phys. Rev. B **101**, 014411 (2020).

[10] A. Smith, M. S. Kim, F. Pollmann, and J. Knolle, Simulating quantum many-body dynamics on a current digital quantum computer, npj Quantum Inf. **5**, 106 (2019).

[11] N. Keenan, N. Robertson, T. Murphy, S. Zhuk, and J. Goold, Evidence of Kardar-Parisi-Zhang scaling on a digital quantum simulator, arXiv:2208.12243.

[12] D. S. Abrams and S. Lloyd, Quantum algorithm providing exponential speed increase for finding eigenvalues and eigenvectors, Phys. Rev. Lett. **83**, 5162 (1999).

[13] A. Y. Kitaev, Quantum computations: Algorithms and error correction, Russ. Math. Surv. **52**, 1191 (1997).

[14] R. Cleve, A. Ekert, C. Macchiavello, and M. Mosca, Quantum algorithms revisited, Proc. R. Soc. London, Ser. A **454**, 339 (1998).

[15] A. Aspuru-Guzik, A. D. Dutoi, P. J. Love, and M. Head-Gordon, Simulated quantum computation of molecular energies, Science **309**, 1704 (2005).

[16] I. Kassal, J. D. Whitfield, A. Perdomo-Ortiz, M.-H. Yung, and A. Aspuru-Guzik, Simulating chemistry using quantum computers, Annu. Rev. Phys. Chem. **62**, 185 (2011).

[17] M. B. Hastings, D. Wecker, B. Bauer, and M. Troyer, Improving quantum algorithms for quantum chemistry, Quantum Inf. Comput. **15**, 1 (2015).

[18] Y. Cao, J. Romero, J. P. Olson, M. Degroote, P. D. Johnson, M. Kieferová, I. D. Kivlichan, T. Menke, B. Peropadre, N. P. D. Sawaya *et al.*, Quantum chemistry in the age of quantum computing, Chem. Rev. **119**, 10856 (2019).

[19] N. P. de Leon, K. M. Itoh, D. Kim, K. K. Mehta, T. E. Northup, H. Paik, B. S. Palmer, N. Samarth, S. Sangtawesin, and D. W. Steuerman, Materials challenges and opportunities for quantum computing hardware, Science **372**, eabb2823 (2021).

[20] M. Cerezo, A. Arrasmith, R. Babbush, S. C. Benjamin, S. Endo, K. Fujii, J. R. McClean, K. Mitarai, X. Yuan, L. Cincio, and P. J. Coles, Variational quantum algorithms, Nat. Rev. Phys. **3**, 625 (2021).

[21] K. Bharti, A. Cervera-Lierta, T. H. Kyaw, T. Haug, S. Alperin-Lea, A. Anand, M. Degroote, H. Heimonen, J. S. Kottmann, T. Menke, W.-K. Mok, S. Sim, L.-C. Kwek, and A. Aspuru-Guzik, Noisy intermediate-scale quantum algorithms, Rev. Mod. Phys. **94**, 015004 (2022).

[22] K. Temme, T. J. Osborne, K. G. Vollbrecht, D. Poulin, and F. Verstraete, Quantum metropolis sampling, Nature (London) **471**, 87 (2011).

[23] A. N. Chowdhury, and R. D. Somma, Quantum algorithms for Gibbs sampling and hitting-time estimation, Quantum Inf. Comput. **17**, 41 (2017).

[24] J. Cohn, F. Yang, K. Najafi, B. Jones, and J. K. Freericks, Minimal effective Gibbs ansatz: A simple protocol for extracting an accurate thermal representation for quantum simulation, Phys. Rev. A **102**, 022622 (2020).

[25] M. Motta, C. Sun, A. T. K. Tan, M. J. O'Rourke, E. Ye, A. J. Minnich, F. G. S. L. Brandão, and G. K.-L. Chan, Determining eigenstates and thermal states on a quantum computer using quantum imaginary time evolution, Nat. Phys. **16**, 205 (2020).

[26] S. Lu, M. C. Bañuls, and J. I. Cirac, Algorithms for quantum simulation at finite energies, PRX Quantum **2**, 020321 (2021).

[27] A. Schuckert, A. Bohrdt, E. Crane, and M. Knap, Probing finite-temperature observables in quantum simulators with short-time dynamics, arXiv:2206.01756.

[28] A. Weiße, G. Wellein, A. Alvermann, and H. Fehske, The Kernel polynomial method, Rev. Mod. Phys. **78**, 275 (2006).

[29] A. M. Childs, R. Kothari, and R. D. Somma, Quantum algorithm for systems of linear equations with exponentially improved dependence on precision, SIAM J. Comput. **46**, 1920 (2017).

[30] P. Rall, Quantum algorithms for estimating physical quantities using block encodings, Phys. Rev. A **102**, 022408 (2020).

[31] A. Roggero, Spectral-density estimation with the Gaussian integral transform, Phys. Rev. A **102**, 022409 (2020).

[32] A. Rajput, A. Roggero, and N. Wiebe, Hybridized methods for quantum simulation in the interaction picture, Quantum **6**, 780 (2022).

[33] P. W. K. Jensen, P. D. Johnson, and A. A. Kunitsa, A near-term quantum algorithm for computing molecular and materials properties based on recursive variational series methods, Phys. Rev. A **108**, 022422 (2023).

[34] H. Wang, J. Nan, T. Zhang, X. Qiu, W. Chen, and X. Li, Kernel function based quantum algorithms for finite temperature quantum simulation, Phys. Rev. B **108**, 085102 (2023).

[35] J. Hartse and A. Roggero, Faster spectral density calculation using energy moments, Eur. Phys. J. A **59**, 41 (2023).

[36] M. Suzuki, General theory of fractal path integrals with applications to many-body theories and statistical physics, J. Math. Phys. **32**, 400 (1991).

[37] Quantinuum H1-1 system, https://www.quantinuum.com.

[38] F. A. Wolf, I. P. McCulloch, O. Parcollet, and U. Schollwöck, Chebyshev matrix product state impurity solver for dynamical mean-field theory, Phys. Rev. B **90**, 115124 (2014).

[39] Y. Yang, S. Iblisdir, J. I. Cirac, and M. C. Bañuls, Probing thermalization through spectral analysis with matrix product operators, Phys. Rev. Lett. **124**, 100602 (2020).

[40] I. Papaefstathiou, D. Robaina, J. I. Cirac, and M. C. Bañuls, Density of states of the lattice Schwinger model, Phys. Rev. D **104**, 014514 (2021).

[41] F. Jin, D. Willsch, M. Willsch, H. Lagemann, K. Michielsen, and H. D. Raedt, Random state technology, J. Phys. Soc. Jpn. **90**, 012001 (2021).

[42] E. Knill and R. Laflamme, Power of one bit of quantum information, Phys. Rev. Lett. **81**, 5672 (1998).

[43] Namely, a control unitary operator applied between two Hadamard operators.

[44] A. Ambainis, L. J. Schulman, and U. Vazirani, Computing with highly mixed states, arXiv:quant-ph/0003136.

[45] A. Datta, Studies on the role of entanglement in mixed-state quantum computation, arXiv:0807.4490.

[46] T. Morimae, K. Fujii, and J. F. Fitzsimons, Hardness of classically simulating the one-clean-qubit model, Phys. Rev. Lett. **112**, 130502 (2014).

[47] K. Fujii, H. Kobayashi, T. Morimae, H. Nishimura, S. Tamate, and S. Tani, Impossibility of classically simulating one-clean-qubit model with multiplicative error, Phys. Rev. Lett. **120**, 200502 (2018).

[48] S. Boixo, S. V. Isakov, V. N. Smelyanskiy, R. Babbush, N. Ding, Z. Jiang, M. J. Bremner, J. M. Martinis, and H. Neven, Characterizing quantum supremacy in near-term devices, Nat. Phys. **14**, 595 (2018).

[49] M. A. Nielsen and I. L. Chuang, *Quantum Computation and Quantum Information: 10th Anniversary Edition* (Cambridge University Press, Cambridge, 2010).

[50] J. Emerson, Y. S. Weinstein, M. Saraceno, S. Lloyd, and D. G. Cory, Pseudo-random unitary operators for quantum information processing, Science **302**, 2098 (2003).

[51] A. Ambainis and J. Emerson, Quantum t designs: t-wise independence in the quantum world, in *Twenty-Second Annual IEEE Conference on Computational Complexity (CCC'07)* (IEEE, 2007), p. 129.

[52] Y. Nakata, D. Zhao, T. Okuda, E. Bannai, Y. Suzuki, S. Tamiya, K. Heya, Z. Yan, K. Zuo, S. Tamate, Y. Tabuchi, and Y. Nakamura, Quantum circuits for exact unitary t designs and applications to higher-order randomized benchmarking, PRX Quantum **2**, 030339 (2021).

[53] In some particular cases, it has been proven that the pseudorandom states after a certain depth become T designs [91].

[54] J. Richter and A. Pal, Simulating hydrodynamics on noisy intermediate-scale quantum devices with random circuits, Phys. Rev. Lett. **126**, 230501 (2021).

[55] L. Coopmans, Y. Kikuchi, and M. Benedetti, Predicting Gibbs-state expectation values with pure thermal shadows, PRX Quantum **4**, 010305 (2023).

[56] K. Seki and S. Yunoki, Energy-filtered random-phase states as microcanonical thermal pure quantum states, Phys. Rev. B **106**, 155111 (2022).

[57] S. Goto, R. Kaneko, and I. Danshita, Matrix product state approach for a quantum system at finite temperatures using random phases and Trotter gates, Phys. Rev. B **104**, 045133 (2021).

[58] S. Goto, R. Kaneko, and I. Danshita, Evaluating thermal expectation values by almost ideal sampling with Trotter gates, Phys. Rev. B **107**, 024307 (2023).

[59] J. M. Pino, J. M. Dreiling, C. Figgatt, J. P. Gaebler, S. A. Moses, M. S. Allman, C. H. Baldwin, M. Foss-Feig, D. Hayes, K. Mayer, C. Ryan-Anderson, and B. Neyenhuis, Demonstration of the trapped-ion quantum CCD computer architecture, Nature (London) **592**, 209 (2021).

[60] We point out that $\hat{Z}$ can be virtually implemented independently of the device, as it commutes or anticommutes with all the gates.

[61] D. N. Page, Average entropy of a subsystem, Phys. Rev. Lett. **71**, 1291 (1993).

[62] G. Brassard, P. Høyer, M. Mosca, and A. Tapp, Quantum amplitude amplification and estimation, in *Quantum Computation and Information* (American Mathematical Society, 2002), p. 53.

[63] E. Campbell, Random compiler for fast Hamiltonian simulation, Phys. Rev. Lett. **123**, 070503 (2019).

[64] C.-F. Chen, H.-Y. Huang, R. Kueng, and J. A. Tropp, Concentration for random product formulas, PRX Quantum **2**, 040305 (2021).

[65] P. K. Faehrmann, M. Steudtner, R. Kueng, M. Kieferova, and J. Eisert, Randomizing multi-product formulas for Hamiltonian simulation, Quantum **6**, 806 (2022).

[66] D. W. Berry, A. M. Childs, Y. Su, X. Wang, and N. Wiebe, Time-dependent Hamiltonian simulation with l^1-norm scaling, Quantum **4**, 254 (2020).

[67] A. M. Childs and N. Wiebe, Hamiltonian simulation using linear combinations of unitary operations, Quantum Inf. Comput. **12**, 901 (2012).

[68] D. W. Berry, A. M. Childs, R. Cleve, R. Kothari, and R. D. Somma, Simulating Hamiltonian dynamics with a truncated Taylor series, Phys. Rev. Lett. **114**, 090502 (2015).

[69] D. W. Berry, A. M. Childs, and R. Kothari, Hamiltonian simulation with nearly optimal dependence on all parameters, in *2015 IEEE 56th Annual Symposium on Foundations of Computer Science* (IEEE, 2015), pp. 792–809.

[70] G. H. Low and I. L. Chuang, Optimal Hamiltonian simulation by quantum signal processing, Phys. Rev. Lett. **118**, 010501 (2017).

[71] G. H. Low and I. L. Chuang, Hamiltonian simulation by qubitization, Quantum **3**, 163 (2019).

[72] Y. Kikuchi, C. M. Keever, L. Coopmans, M. Lubasch, and M. Benedetti, Realization of quantum signal processing on a noisy quantum computer, arXiv:2303.05533.

[73] A. M. Childs, D. Maslov, Y. Nam, N. J. Ross, and Y. Su, Toward the first quantum simulation with quantum speedup, Proc. Natl. Acad. Sci. USA **115**, 9456 (2018).

[74] A. M. Childs, Y. Su, M. C. Tran, N. Wiebe, and S. Zhu, Theory of Trotter error with commutator scaling, Phys. Rev. X **11**, 011020 (2021).

[75] G. García-Pérez, M. A. C. Rossi, B. Sokolov, F. Tacchino, P. K. Barkoutsos, G. Mazzola, I. Tavernelli, and S. Maniscalco, Learning to measure: Adaptive informationally complete generalized measurements for quantum algorithms, PRX Quantum **2**, 040342 (2021).

[76] H.-Y. Huang, R. Kueng, and J. Preskill, Predicting many properties of a quantum system from very few measurements, Nat. Phys. **16**, 1050 (2020).

[77] K. Mitarai and K. Fujii, Methodology for replacing indirect measurements with direct measurements, Phys. Rev. Res. **1**, 013006 (2019).

[78] A. Schuckert, A. Bohrdt, E. Crane, and M. Knap, Probing finite-temperature observables in quantum simulators of spin systems with short-time dynamics, Phys. Rev. B **107**, L140410 (2023).

[79] V. Balachandran, L. F. Santos, M. Rigol, and D. Poletti, Slow relaxation of out-of-time-ordered correlators in interacting integrable and nonintegrable spin-$\frac{1}{2}$ XYZ chains, Phys. Rev. B **107**, 235421 (2023).

[80] M. Hartmann, G. Mahler, and O. Hess, Spectral densities and partition functions of modular quantum systems as derived from a central limit theorem, J. Stat. Phys. **119**, 1139 (2005).

[81] J. P. Boyd, *Chebyshev & Fourier Spectral Methods*, Lecture Notes in Engineering (Springer, Berlin, 1989).

[82] G. Meinardus, *Approximation of Functions: Theory and Numerical Methods* (Springer, Berlin, 1967).

[83] D. Poulin and P. Wocjan, Sampling from the thermal quantum Gibbs state and evaluating partition functions with a quantum computer, Phys. Rev. Lett. **103**, 220502 (2009).

[84] E. Bilgin and S. Boixo, Preparing thermal states of quantum systems by dimension reduction, Phys. Rev. Lett. **105**, 170405 (2010).

[85] M.-H. Yung and A. Aspuru-Guzik, A quantum-quantum metropolis algorithm, Proc. Natl. Acad. Sci. USA **109**, 754 (2012).

[86] C.-F. Chen, M. J. Kastoryano, F. G. S. L. Brandão, and A. Gilyén, Quantum thermal state preparation, arXiv:2303.18224.

[87] S.-N. Sun, M. Motta, R. N. Tazhigulov, A. T. K. Tan, G. K.-L. Chan, and A. J. Minnich, Quantum computation of finite-temperature static and dynamical properties of spin systems using quantum imaginary time evolution, PRX Quantum **2**, 010317 (2021).

[88] S. R. White, Minimally entangled typical quantum states at finite temperature, Phys. Rev. Lett. **102**, 190601 (2009).

[89] K. Seki and S. Yunoki, Quantum power method by a superposition of time-evolved states, PRX Quantum **2**, 010333 (2021).

[90] K. Wan, M. Berta, and E. T. Campbell, Randomized quantum algorithm for statistical phase estimation, Phys. Rev. Lett. **129**, 030503 (2022).

[91] A. Harrow and S. Mehraban, Approximate unitary t-designs by short random quantum circuits using nearest-neighbor and long-range gates, arXiv:1809.06957.